This is a pre-copyedited, author-produced version of an article accepted for publication in Briefings in Bioinformatics following peer review. The version of record Rajesh Pal, Amit Kumar, Gauri Misra, Exploring TEAD2 as a drug target for therapeutic intervention of cancer: A multi-computational case study, Briefings in Bioinformatics, Volume 22, Issue 5, September 2021, bbab007 is available online at: https://academic.oup.com/bib/article/22/5/bbab007/6145134?login=true , https://doi.org/10.1093/bib/bbab007

Exploring TEAD2 as a drug target for therapeutic intervention of cancer: A multi-computational case study

Rajesh Pal[†] , Amit Kumar[†] and Gauri Misra

Corresponding author: Dr Gauri Misra, National Institute of Biologicals, A-32, Institutional Area, Block-A, Industrial Area, Sector-62, Noida-201309, Uttar Pradesh, India. E-mail: kamgauri@gmail.com
[†]These authors contributed equally.

Abstract

Transcriptional enhanced associate domain (TEAD) is a family of transcription factors that plays a significant role during embryonic developmental processes, and its dysregulation is responsible for tumour progression. TEAD is considered as druggable targets in various diseases, namely cancer, cardiovascular diseases and neurodegenerative disorders. Previous structural studies revealed the importance of the central hydrophobic pocket of TEAD as a potential target for small-molecule inhibitors and demonstrated flufenamic acid (FLU) (a COX-2 enzyme inhibitor) to bind and inhibit TEAD2 functions. However, to date, no drug candidates that bind specifically to TEAD2 with high selectivity and efficacy have been developed or proposed. Within this framework, we present here a case study where we have identified potential TEAD2 inhibitor candidates by integrating multiple computational approaches. Among the candidates, the top two ranked compounds ZINC95969481 (LG1) which is a fused pyrazole derivative and ZINC05203789 (LG2), a fluorene derivative resulted in much favourable binding energy scores than the reference ligand, FLU. The drug likeliness of the best compounds was also evaluated *in silico* to ensure the bioavailability of these compounds particularly LG1 as compared to FLU thus providing a strong rationale for their development as leads against TEAD. Molecular dynamics simulations results highlighted the role of key residues contributing to favourable interactions in TEAD2-LG1 complex with much favourable interaction and binding free energy values with respect to the reference compound. Altogether, this study provides a starting platform to be more exploited by future experimental research towards the development of inhibitors against TEAD, a persuasive strategy for therapeutic intervention in cancer treatment.

Gauri Misra is a senior scientist (II) presently working at the National Institute of Biologicals, Noida (an Autonomous Institute under the Ministry of Health and Family Welfare, Government of India) with expertise in Structural Biology and Bioinformatics.
Rajesh Pal is a PhD student in the Department of Biomedical Sciences, University of Cagliari. He has been working on NGS approaches to understand the metagenesis of hepatocellular carcinoma.
Amit Kumar is a postdoctoral fellow in the Department of Electrical and Electronic Engineering, University of Cagliari. His research focuses on the modelling of biologically relevant protein-ligand structures and their dynamics.
Submitted: 16 September 2020; **Received (in revised form):** 30 November 2020

Graphical Abstract

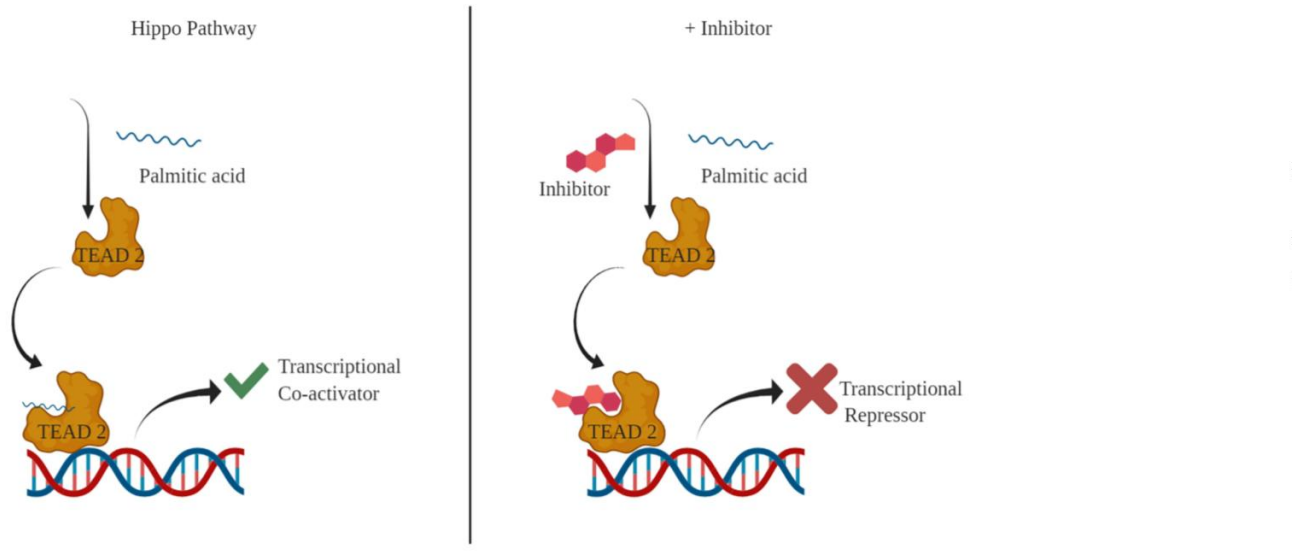

Key words: transcriptional enhanced associate domain (TEAD); drug discovery; molecular dynamics (MD); flufenamic acid (FLU); pharmacophore model; ADMET analysis

Introduction

The transcriptional enhanced associate domain (TEAD) family of transcription factors were discovered in an attempt to identify the nuclear proteins that could bind SV40 enhancer and activate transcription [1]. They are widely studied in the context of the regulation of Hippo signalling pathway. TEAD1 was the first transcription factor of the family that was identified. Further studies have revealed that TEAD also binds to human HPV-16 oncogenes and M-CAT motifs [2, 3]. TEAD family is evolutionary conserved consisting of a highly conserved DNA binding domain with a consensus sequence 5′-CATTCCA/T-3′ referred to as the MCAT element [4]. TEAD family members are known to play critical roles in various biological processes and human diseases.

Four TEAD genes (TEAD 1–4) are expressed in mammals and each TEAD regulates a tissue-specific expression, signifying specific roles for each member. TEADs have significant roles in development, with specific roles at the two-cell embryo stage and cardiogenesis [5], neural crest [6] and notochord development [7], and Trophectoderm lineage determination [8].

TEADs are primary transcriptional factors that require the presence of Yes associated protein (YAP)/TAZ transcription coactivators to induce target gene transcription [9]. The transcriptional activity of TEAD is regulated by the presence or absence of nuclear YAP/transcriptional activator with PDZ binding domain (TAZ) in the Hippo pathway. YAP/TAZ on phosphorylation by large tumour suppressor kinase LATS1/2 is localized in the cytoplasm and becomes incapable of binding to TEAD thus making it transcriptionally inactive. After dephosphorylation, YAP/-TAZ is translocated to the nucleus where they bind to TEAD and lead to transcription of target genes which are critical for cell growth, proliferation and survival [10–12]. Structural studies have revealed that the TEAD binding domain of YAP is located in the N terminus of the protein, and the YAP binding domain is present at the C terminal transactivation domain of TEAD. One molecule each of YAP and TEAD binds to form a heterodimer complex. The N terminal of YAP wraps around the globular C terminal structure of TEAD using three major interfaces [13, 14]. The residues that are critical for interaction are evolutionarily conserved on both TEAD and YAP [14]. The binding of TAZ and TEAD displays two conformations; (i) one molecule each of TAZ and TEAD binds to form a heterodimer, similar to that of YAP and TEAD, (ii) two molecules each of TAZ and TEAD bind besides, the two TAZ molecules that interacts with each other to bridge two TEAD molecules, forming a heterotetrameric complex [15]. Human interactome studies have also shown interaction between the TEADs, suggesting that homocomplexes and heterocomplexes may regulate the transcriptional activity of TEAD differentially [16, 17].

The role of Hippo signalling in the development of cancer is well studied, and this development is a consequence of YAP/TAZ amplification and hyperactivity in many cancers [18].

Interestingly, increased expression and activity of TEAD, both dependent and independent of YAP/TAZ, has also been implicated in the progression of several solid tumours [19]. The expression levels of TEAD which is high in prostate [20], colorectal [21] and breast cancers [22] is an indicator of poor clinical outcome. TEAD4 is significantly overexpressed in metastatic tissues of colorectal cancer and its *in vitro* and *in vivo* knockdown leads to reduction in cell migration and metastasis [21]. Also, the increase in metastatic potential in colorectal cancer is YAP independent. TEAD1 is known to play

a role in conferring resistance to apoptosis, independent of YAP [23]. TEAD1 is also known to regulate mesothelin, a gene that acts as a cancer biomarker due to its overexpression in various tumours [24]. Furthermore, it has been shown that binding of YAP/TAZ-TEAD and AP-1 to enhancers, together activates the target genes that are important for oncogenic growth, invasion and metastasis [25, 26]. TEADs are also known to promote the transcriptional activity responsible for increased invasiveness and resistance to mitogen activated protein kinase (MAPK) inhibition in melanomas [27].

Structural studies of TEAD have identified a central hydrophobic pocket in the transactivation domain [28]. The binding of Flufenamate drug in the hydrophobic pocket of TEAD inhibits its transcriptional activity without disrupting the YAP-TEAD interaction, which leads to a decrease in cell migration and proliferation [28]. In this hydrophobic pocket of TEAD, palmitoylation occurs, indicating that Flufenamate drugs, despite having a low binding affinity, may inhibit TEAD activity by removing TEAD palmitoylation [29, 30]. In YAP/TAZ driven cancers, disruption of YAP/TAZ-TEAD interaction by treatment with a VGLL4 mimicking peptide inhibits gastric cancer growth both *in vitro* and *in vivo* thus outcompeting YAP for TEAD binding [31]. Verteporfin, a small-molecule inhibitor known to inhibit YAP-TEAD interaction also suppresses cancer cell growth [32]. These studies have successfully established roles of TEADs in cancer development and progression, thus indicating TEAD as critical drug targets that can be exploited for cancer therapy.

The development of inhibitors against TEAD is a potent strategy for therapeutic intervention in cancer treatment. Previous biochemical studies have demonstrated that flufenamates bind and inhibit TEAD functions, highlighting the necessity for affinity optimization of drug candidates against TEAD protein. Therefore, the exploration of drug candidates that specifically bind the central TEAD hydrophobic pocket with high selectivity and efficacy is crucial. In this scenario, the present study aims to identify potential inhibitors of TEAD using multi-computational strategies involving virtual screening (VS), ligand-based pharmacophore modelling, docking, and molecular dynamics (MD) simulations.

Materials and methods

Protein preparation and grid generation

The crystal structure used for the protein was obtained from protein data bank (PDB:5DQ8). Prior to docking experiment, the protein structure was pre-processed using Schrodinger's protein preparation Wizard [33] tool (Maestro, version 11) by assigning the bond orders to all the bonds in the structure. Chemical components dictionary database was used to assign bond orders to the het groups in the structure. The missing hydrogen atoms were added and formal charge was corrected on the metal and neighbouring atoms. Disulphide bonds were created between sulphur atoms within 3.2 Å. For heteroatoms,probable ionization and tautomeric states were generated in the pH range 7.0 ± 2.0. After preparation and refinement of the protein structure, the grid was generated around the ligand flufenamic acid (FLU) reported in the crystal structure (PDB:5DQ8) with receptor grid generation using Glide module [34–36]. Some of the methods for ligand and protein preparation were adapted from our previous studies [37–39]. Docking accuracy was confirmed using blind docking. The ligand was prepared again and redocked in the protein. Root mean square (RMS) deviation between reported conformation and docked conformation of the ligand was calculated to be 0.2 Å, which was within the acceptable limits.

Ligand preparation

All the compounds were prepared using Ligprep (Maestro, version 11) module in Schrodinger. Possible ionization states were generated within the pH range of 7.0 ± 2.0 using Epik program. Desalt option was selected to retain the largest molecule in the workspace and thus removing the counter ions or water molecules. Tautomer's were generated for each molecule in the workspace. Stereoisomers were generated at most 32 per ligand by retaining the specified chiralities from the input file.

Pharmacophore hypothesis generation, enrichment calculation and database screening

After protein preparation, all the ligand interactions were scrutinized. Within the 4 Å distance, FLU mostly formed hydrophobic interactions. It also formed a hydrogen bond between the carboxylate group and main chain amide nitrogen of C380. Salt bridge interactions were also observed between the carboxylate group and K357. The benzoic acid part of the FLU was in contact with residues S345, V355, V329, V347, C380, M379 and K357. The fluorine's in FLU interacted with the hydrophobic residues, namely A235, V252, F428, F233 and L383. Additionally, other regions of the Trifluoromethyl-benzene ring also interacted with residues I408, L383, F233 and Q410.

Based on the binding characteristics of FLU, a 3D ligand-based pharmacophore hypothesis was developed. The pharmacophore model was built using the Phase module of Schrodinger. Default hypothesis settings were used for receptor-based excluded volume shell.

Prior to VS, the pharmacophore model was evaluated using Enrichment calculator tool of the Schrodinger suite. A set of compounds with known activity (true-positives) and a decoy set (false positives) consisting of inactive compounds were used. In our study Niflumic acid, FLU, and Bromo-fenamic acid were considered as actives, as they were reported to be analogues that bind to the protein pocket in similar manner.

A total of 8 396 000 commercially available ligands were downloaded from the ZINC database. The database consisted of well-known chemical catalogues from Enamine, Molport, Asinex and Sigma–Aldrich. Before docking, ligands were screened against the final hypothesis. Ligands having fitness score >1.5 were further taken into consideration.

Virtual screening/molecular docking

A total of 5000 ligands having fitness score >1.5 were subjected to molecular docking. Docking was carried out using the VS workflow of Glide Module. The workflow included ligand preparation, filtering based on properties grid generation and up to three docking stages progressing from HTVS (high throughput VS) to SP (standard precision) to XP (extra precision) docking.

Absorption, distribution, metabolism, and excretion calculations

Absorption, distribution, metabolism and excretion (ADME) are important pharmacokinetic parameters for establishing the drug likeliness of any compound. These properties were calculated using the QikProp [40] module of Schrodinger (Maestro, version 11) using default molecular descriptors.

MD simulation

The compounds having high glide score and high fitness score were subjected to MD simulations. All simulations were performed using NAMD (2.8 version) software package [41], and using Amber ff99SB force field parameters. The starting protein-ligand complex structure represents the best ligand pose predicted from the docking procedure. Each complex was built using the tleap module of Amber 11 software package, followed by solvation in an explicit water box with a minimum distance between any atom of the complex and edge of the box of 20 Å. Standard MD protocols such as minimization and gradual heating of the system were done to 300 K, with initial positional restraints on the carbon-alpha atoms of the protein [42, 43]. Gradually, the positional restraints were released during the simulation time, followed by an equilibration run of 10 ns at 300 K. We performed 100 ns production run for each system with 2 fs time step, resulting in total of 300 ns, in NPT ensemble using periodic boundary conditions. Particle mesh Ewald scheme [44] was used to estimate long-range electrostatic interactions and a cut-off radius 12 Å was employed for the non-bonded interactions. MD simulation data analysis was performed using grcarma [45], sietraj [46] and vmd (version 1.9.3) [47] software packages.

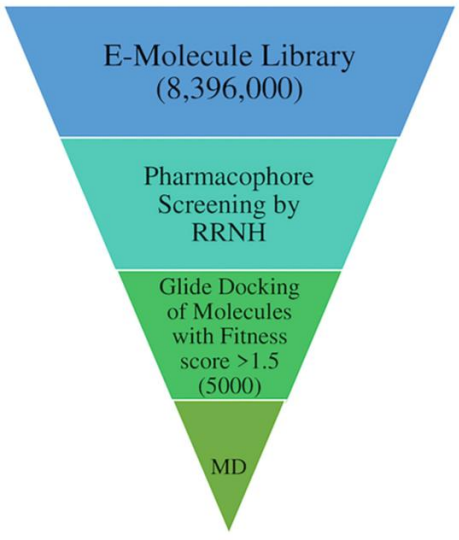

Figure 1. Computational workflow.

Results and discussion

TEAD proteins are the important class of transcription factors that are crucial in the development of human cancers. Recent studies have demonstrated the major role of TEAD and interacting coactivators in the progression of various cancers such as Glioblastoma, liver and ovarian cancers. They promote cancer progression through genes involved in cell proliferation. Thus, under oncogenic conditions, antagonizing hippo transcription by targeting TEAD proteins has emerged as a promising therapeutic target. In 2015, Pobbati *et al*. reported the TEAD2 crystal structure in complex with FLU (5DQ8) and bromo-fenamic acid (5DQE). FLU and bromo-fenamic acid were identified using fragment-based screening method and both of them targeted the central hydrophobic pocket. Fragment-based screening is a popular method applied for the discovery of the lead molecules. Hence, our study focused on identifying potential lead compounds based on the structural properties of FLU. The experimental workflow leading to the identification of the potential leads against TEAD protein is illustrated in Figure 1.

Pharmacophore hypothesis generation

Our final hypothesis consisted of four features as shown in Figure 2 namely RRNH (R- Aromatic Ring, N- Negatively charged group and H- Hydrophobic group). In detail, the hypothesis consisted of aromatic rings of phenyl and benzoic acid, which formed important hydrophobic interactions with the protein. It also included the carboxylate group present at benzoic acid, and trifluoromethyl group which exhibited interactions with the hydrophobic protein residues.

Various metrics such as the average rank of actives, the enrichment factor (EF), the area under the receiver operating characteristic curve (ROC), Boltzmann-enhanced discrimination of receiver operating characteristic (BEDROC), the area under the accumulation curve (AUAC), were used to evaluate the performance of the pharmacophore model. In order to determine the robustness of the hypothesis robust initial enhancement (RIE) scores were also taken in to consideration (Table 1).

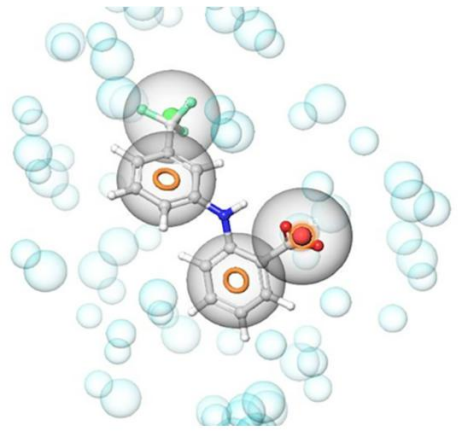

Figure 2. Final Pharmacophore Hypothesis Model (RRNH). Grey spheres showing the important features selected during hypothesis development and blue spheres representing the volume shell.

Enrichment results indicated that the screening protocol was extremely good at retrieving the active compounds from the decoy set. Three out of three ranked actives were retrieved with remarkable ROC of (1.00), AUAC (1.00), RIE (19.41) and a high EF of 1e+02 at 1% of sample size. The high value of BEDROC at alpha = 20.0, alpha = 160.9 and alpha = 8.0 indicates the early identification of actives among the compound database.

Table 1. Validation parameters

S. No	Parameters	Values
1.	Number of actives (1%; 2%; 5%; 10%; 20%)	3,3,3,3,3
2.	% of actives (1%; 2%; 5%; 10%; 20%)	100.0, 100.0, 100.0. 100.0. 100.0
3.	EF (1%; 2%; 5%; 10%; 20%)	1e+02, 50, 20, 10,5
4.	ROC	1.00
5.	RIE	19.41
6.	AUAC	1.00
7.	BEDROC (alpha = 20.0; 160.9)	1.000, 1.000, 1.000

Table 2. Comparison of binding energy (docking) scores between flufenamic acid and two best ligands obtained through virtual screening

ZINC ID	Dock Score/Glide Score (kcal/mol)	MMGBSA (kcal/mol)	Molecular Weight (g/mol)	Number of hydrogen bonds	Fitness score
Flufenamic acid	−10.69	−63.82	281.23	1	–
ZINC95969481	−14.5	−54.2	407.3	2	1.5
ZINC05203789	−13.8	−42.8	357.3	1	1.9

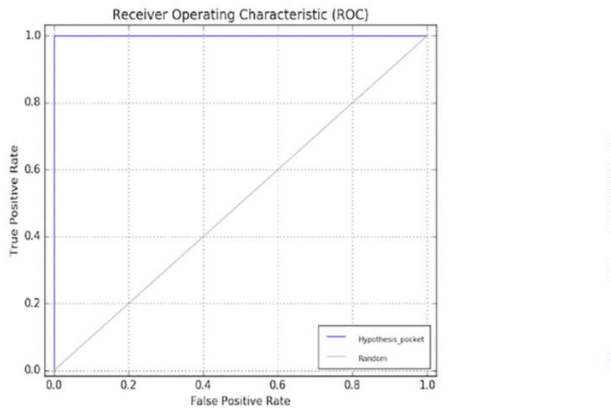

Figure 3. Receiver operating characteristic (ROC) curve for RRNH hypothesis.

Receiver operating characteristics

The ROC curve allows visualization of the performance of the hypothesis in discriminating power to correctly identify the active ligands from a decoy set. Accuracy is measured by the area under the curve [48, 49]. The ROC plot for RRNH hypothesis is represented in Figure 3. An area of 1 denotes a perfect test, whereas an area of 0.5 denotes a poor test while evaluation. The ROC for the RRNH hypothesis was calculated to be 1, clearly indicative of model accuracy with a high chance of screening active molecules 100% effectively from the decoy set.

VS/molecular docking

A total of 8 396 000 molecules were screened from the Zinc15 database (last access: 24 August 2020) and a total of 53 ligands were found with glide scores >-7 kcal/mol (supplementary information). In Table 2, we report the docking scores of reference ligand FLU and the two best identified ligands.

Based on binding energy scores, the top two ranked candidates are ZINC95969481 (LG1) with IUPAC name 1-{1-[3-(trifluoromethyl) phenyl]-1H,4H,5H,6H-cyclopenta[c]pyrazole-3-carbonyl} piperidine-3-carboxylic acid, a fused pyrazole derivative, and ZINC05203789 (LG2) with IUPAC name (2R)-2-[(9-oxo-9H-fluoren-4-yl) formamido]-2-phenylacetic acid, a fluorene derivative. Previous studies have investigated a wide range of drug-like properties of pyrazole derivatives along with their physiological and pharmacological activities, which showed that this class of compounds can be targeted for the discovery of new drugs [50]. Recently fused pyrazole derivatives have been reported as EGFR and VEGFR-2 dual TK inhibitors [51–53].

The two ligands (LG1, LG2) bound preferentially to the same site (Figure 4A and B) as the reference ligand FLU and shared contacts involving the carboxyl functional group (COO^-) with residue Cys380. The top-ranked compound (LG1) displayed the best binding energy score, with ∼24% better score value than the reference FLU ligand. In detail, we observed hydrogen bonded interaction between the carbonyl group of compound LG1 with the backbone of Glu410 residue, and a salt bridge interaction involving the piperidine ring and the sidechain of residue Lys357 (Figure 4C).

Compound LG2 displayed a lower docking score (∼5%) with respect to LG1. The fluoren ring of LG2 formed pi–pi interaction with the side chain of residue Phe 428. Notably, the phenyl ring of the phenylacetic acid scaffold of LG2 displayed pi–cation interaction with the side chain of Lys357, and the carboxyl functional group formed a hydrogen bond with the backbone of residue Cys380 and salt bridge interaction with the side chain of Lys 357 (Figure 4D).

In silico ADME prediction

ADME properties were determined for FLU and the top two compounds ZINC95969481 and ZINC05203789 thus saving both time and money during the long drug discovery process. The QikProp has the advantage of using the entire three-dimensional structure of target protein in place of fragment-based approach. Our top-ranked compound ZINC95969481 was predicted to have better Caco-2 cell permeability (QPPCaco) and better absorption (% oral absorption) than FLU. Other important properties of

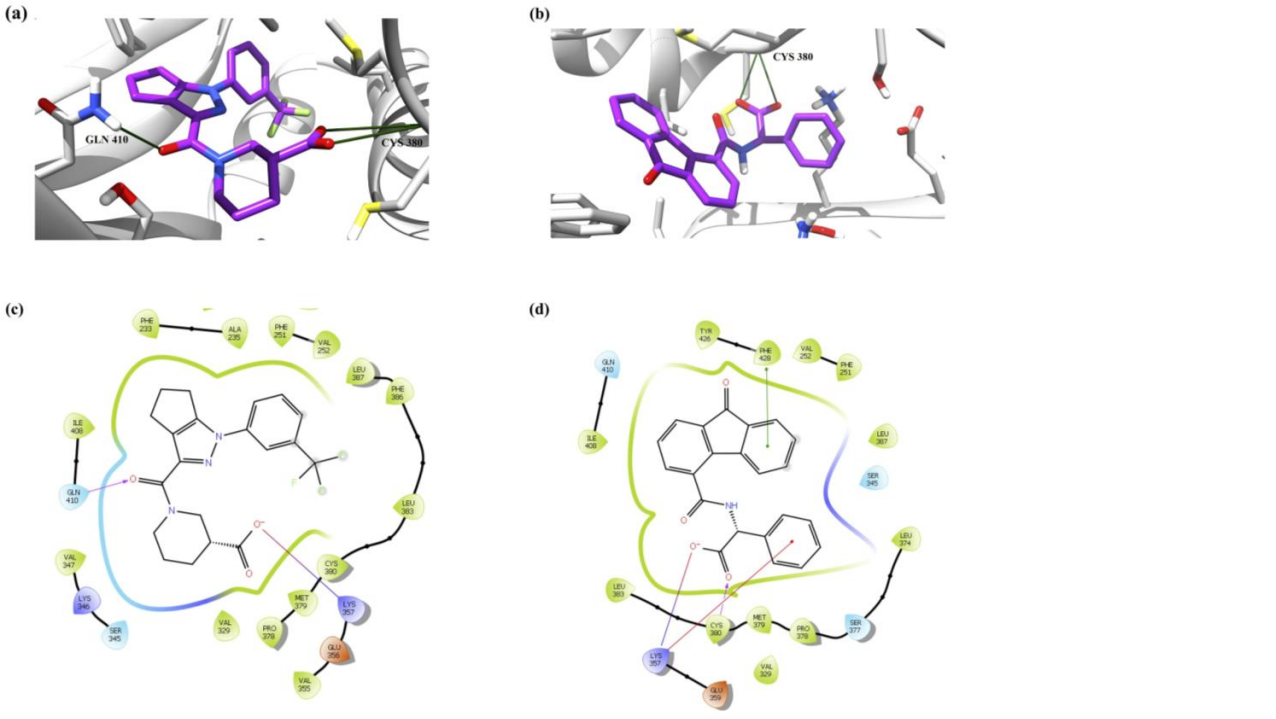

Figure 4. Docked pose and interaction picture of top-ranked ligands. Best-predicted conformation of (A) ZINC95969481 and (B) ZINC05203789. In (C), and (D) interaction picture with the top-ranked ligands.

Table 3. Predicted ADME properties

Compounds	QPlog Po/w	QPlogS	QPPCaco	% oral absorption
Flufenamic acid	5.235	−4.464	272.636	88.206
ZINC95969481	1.120	−2.846	388.110	96.904
ZINC05203789	3.561	−4.877	55.829	79.063
Recommended Values	−2 to 6.5	−6.5 to 0.5	<25 poor >500 great	<25% poor >80% high

the compounds such as predicted octanol/water partition coefficient (QPlog Po/w) and predicted aqueous solubility (QPlogS) are shown in Table 3. Compound ZINC95969481 is better than FLU in all parameters. On the other hand, ZINC05203789 exhibits better QPlog Po/w indicative of octanol/water partition. However, the solubility of the latter compound is as comparable to the FLU. Permeability as observed in Caco cell lines and % oral absorption is lesser than the FLU. Thus, ADMET evaluation is clearly indicative of ZINC95969481 to be a better lead in comparison to FLU that can be experimentally evaluated for its development as a potent inhibitor against TEAD.

MD simulations

Additionally, we have also performed MD simulation of top compounds ZINC95969481 (LG1), ZINC05203789 (LG2), with FLU as control. In order to investigate the relative stability of the ligands residing in the predicted site, MD simulations were performed for the top identified lead compound LG1, intermediate compound LG2, the ligand FLU of the crystal structure.

General stability of the complexes was explored by evaluating MD parameters such as: radius of gyration (Rg), root mean square deviation (rmsd), solvent accessible surface area (SASA) and configurational entropy (Figure 5) along the MD simulation time. Among the ligands, we note slightly higher RMSD and entropy values for LG2, followed by LG1, and FLU, which can be related to higher flexibility of LG2 (four rotatable bond), one more than the top-ranked ligand (LG1). Overall, analysis of the parameters indicated that the MD trajectories are overall stable during the production phase for the four studied complexes.

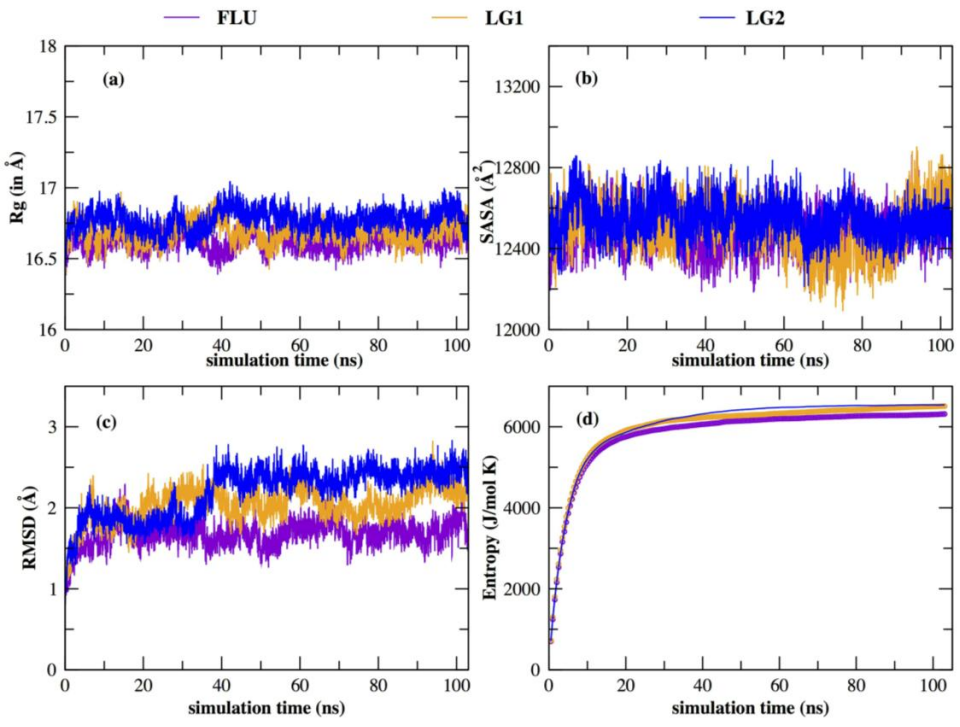

Figure 5. MD parameters over time plot. In (A) radius of gyration (Rg), (B) solvent accessible surface area (SASA), (C) root mean square deviation (RMSD) and (D) configurational entropy for the four ligand complexes.

To further explore the nature of interactions in the binding pockets, hydrogen bonded (H-bond) interactions was evaluated. In Figure 6, persistent H-bond interactions (present at least for 5 ns) are reported. Among the ligands, we note LG1 and LG2 to exhibit higher number of H-bond interactions with respect to the reference ligand FLU. In all the three cases, we found residues Lys 357 and Cys 380 to participate in the H-bond interactions with the ligand. The complexes with LG1 and LG2 ligands showed a shared set of interactions, except that we found H-bond interaction involving Gln 157 to be characteristic to LG1, whereas Ser 124 to LG2.

Subsequently, we calculated non-bonded interaction energy constituting Van der Waals and electrostatic energy between the ligand and the protein residues on 5000 MD snapshots of each system (Figure 7). Among the ligand complexes, we found LG1 complex to display much better (more negative) interaction energy value with respect to the other ligands.

Binding free energy (deltaG) estimation was performed using solvated interaction energy (SIE) approach, which belongs to force field-based scoring functions, of which parameters have been optimized from a dataset of 99 protein-ligand complexes [46]. It allowed a crude but effective treatment of entropy–enthalpy compensation in the binding energy estimation. The average SIE binding free energy value was calculated at a time interval of 20 ps from 100 ns simulation trajectory as shown in Figure 7B. Among three ligands, LG1 displays most favourable binding free energy value (~−10 kcal/mol), whereas other two ligands display around −8 kcal/mol.

A multi-computational approach represents not only a valuable and essential tool in the identification of potential bioactive compounds, but also allows saving resources and time. However, finding an active compound from the shortlisted compounds by employing a fully computational approach remains a challenge. In our study, we have attempted to narrow down the rate of false positives by adopting the ligand-based VS method, which increases the chances of finding novel active compounds. Furthermore, using MD simulations we could estimate binding affinity of the compounds to the TEAD2 protein. Therefore, an experimental validation for the predicted binding affinity of the compounds to TEAD2 remains a limitation of the present study.

Conclusions

In this study, we have presented a multi-computational approach to identify potential candidates against TEAD2 protein, which has been studied as a compelling strategy for therapeutic intervention in the treatment of cancer.

Our study focused on identifying potential candidates based on a ligand-based pharmacophore model consisting of four chemical features (two aromatic rings, a negatively

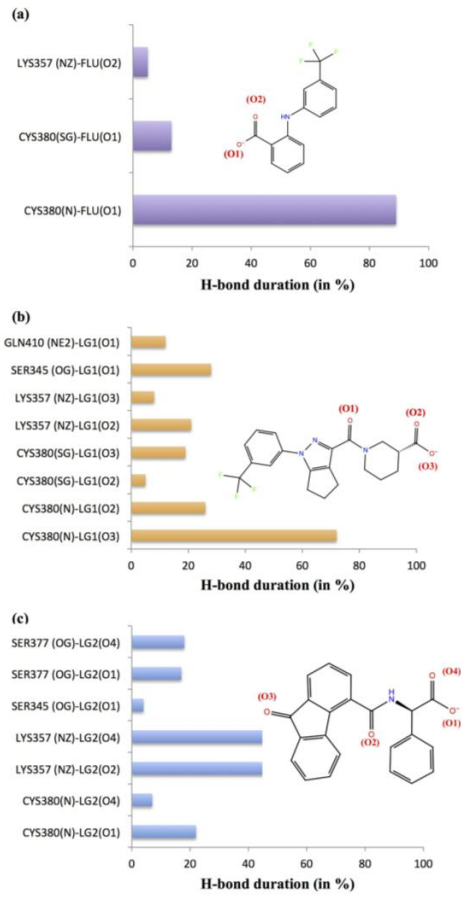

Figure 6. Persistent hydrogen bonded (H-bond) interaction bar plot.

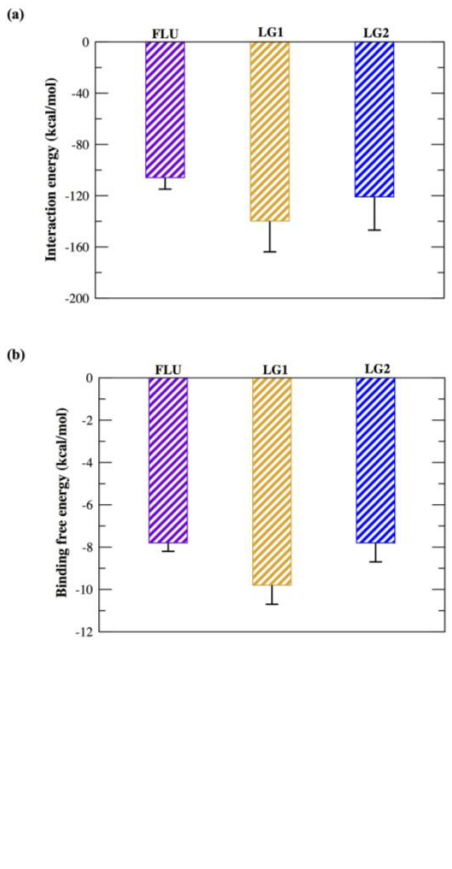

Figure 7. Non-bonded interaction energy and binding free energy plots.

charged functional group and a hydrophobic group), which was generated using FLU.

The pharmacophore model's performance was evaluated using ROC curve, which confirmed the screening protocol to be extremely good at retrieving the active compounds from the decoy set. A total of 8 396 000 molecules were screened from the Zinc database, and a total of 5000 ligands were subjected to the molecular docking process.

The top identified compound, namely ZINC95969481 (LG1), resulting in a binding energy score of −14.5 kcal/mol and with MMGBSA energy score of −54.2 kcal/mol was obtained.To further validate the docking method, MD simulations were performed to examine the stability of the best-predicted conformation for the three protein-ligand complexes. Among the investigated candidates, LG1 exhibited the most favourable interaction energy towards TEAD2 (−140 kcal/mol) and was 32% greater (more negative value) than the reference ligand, FLU. Also, LG1 exhibited better ADME properties as compared to FLU, indicative of its bioavailability during its future experimental validation.

In conclusion, although our in-depth computational investigation establishes compound LG1 as a promising TEAD2 inhibitor candidate, further experimental exploration is needed to confirm our findings. Moreover, exploration of the effect of the best inhibitors on other TEAD isoforms will be the future course of expansion of the present study.

Key Points

- Transcriptional enhanced associate domain (TEAD) is a family of transcription factors that plays a significant role during embryonic developmental processes, and its dysregulation is responsible for tumour progression.
- TEAD2 is an important drug target in various diseases, particularly in cancer. Flufenamic acid (FLU) (a COX-2 enzyme inhibitor) is reported as the inhibitor of TEAD2.
- Present study identifies new more potent inhibitors of TEAD2 in comparison to FLU using multi-computational approaches.
- Effectiveness of new leads against TEAD2 have been validated using molecular dynamics (MD) simulations and ADMET analysis.
- These inhibitors against TEAD are an effective strategy for therapeutic intervention in cancer treatment.

Supplementary data

Supplementary data are available online at https://academic.oup.com/bib.

Acknowledgement

Authors also acknowledge the use of computational resources of Amity University, Noida and Center for Advanced Studies, Research and Development in Sardinia (CRS4). Special thanks to Marco Moro, Michele Muggiri and Carlo Podda for high-performance computing (HPC) support.

Funding

Indian Council of Medical Research (ICMR) (Project Id: 2019-3182 to G.M.).

References

1. Xiao JH, Davidson I, Ferrandon D, *et al*. One cell-specific and three ubiquitous nuclear proteins bind in vitro to overlapping motifs in the domain B1 of the SV40 enhancer. *EMBO J* 1987.
2. Davidson I, Xiao JH, Rosales R, *et al*. The HeLa cell protein TEF-1 binds specifically and cooperatively to two SV40 enhancer motifs of unrelated sequence. *Cell* 1988. doi: 10.1016/0092-8674(88)90108-0.
3. Ishiji T, Lace MJ, Parkkinen S, *et al*. Transcriptional enhancer factor (TEF)-1 and its cell-specific co-activator activate human papillomavirus-16 E6 and E7 oncogene transcription in keratinocytes and cervical carcinoma cells. *EMBO J* 1992;**11**:2271–81.
4. Farrance IKG, Mar JH, Ordahl CP. M-CAT binding factor is related to the SV40 enhancer binding factor, TEF-1. *J Biol Chem* 1992;**267**(24):17234–40.
5. Chen Z, Friedrich GA, Soriano P. Transcriptional enhancer factor 1 disruption by a retroviral gene trap leads to heart defects and embryonic lethality in mice. *Genes Dev* 1994. doi: 10.1101/gad.8.19.2293.
6. Kaneko KJ, Kohn MJ, Liu C, *et al*. Transcription factor TEAD2 is involved in neural tube closure. *Genesis* 2007. doi: 10.1002/dvg.20330.
7. Sawada A, Kiyonari H, Ukita K, *et al*.Redundant roles of Tead1 and Tead2 in notochord development and the regulation of cell proliferation and survival. *Mol Cell Biol* 2008. doi: 10.1128/MCB.01759-07.
8. Yagi R, Kohn MJ, Karavanova I, *et al*. Transcription factor TEAD4 specifies the trophectoderm lineage at the beginning of mammalian development. *Development* 2007. doi: 10.1242/dev.010223.
9. Xiao JH, Davidson I, Matthes H, *et al*. Cloning, expression, and transcriptional properties of the human enhancer factor TEF-1. *Cell* 1991. doi: 10.1016/0092-8674(91)90088-G.
10. Zhao B, Ye X, Yu J, *et al*. TEAD mediates YAP-dependent gene induction and growth control. *Genes Dev* 2008. doi: 10.1101/gad.1664408.
11. Lai D, Ho KC, Hao Y, *et al*. Taxol resistance in breast cancer cells is mediated by the hippo pathway component TAZ and its downstream transcriptional targets Cyr61 and CTGF. *Cancer Res* 2011. doi: 10.1158/0008-5472.CAN-10-2711.
12. Lei Q-Y, Zhang H, Zhao B, *et al*. TAZ promotes cell proliferation and epithelial-mesenchymal transition and is inhibited by the hippo pathway. *Mol Cell Biol* 2008. doi: 10.1128/MCB.01874-07.
13. Chen L, Chan SW, Zhang X, *et al*. Structural basis of YAP recognition by TEAD4 in the hippo pathway. *Genes Dev* 2010. doi: 10.1101/gad.1865310.
14. Li Z, Zhao B, Wang P, *et al*. Structural insights into the YAP and TEAD complex. *Genes Dev* 2010. doi: 10.1101/gad.1865810.
15. Kaan HYK, Chan SW, Tan SKJ, *et al*. Crystal structure of TAZ-TEAD complex reveals a distinct interaction mode from that of YAP-TEAD complex. *Sci Rep* 2017. doi: 10.1038/s41598-017-02219-9.
16. Huttlin EL, Bruckner RJ, Paulo JA, *et al*. Architecture of the human interactome defines protein communities and disease networks. *Nature* 2017. doi: 10.1038/nature22366.
17. Huttlin EL, Ting L, Bruckner RJ, *et al*. The BioPlex network: a systematic exploration of the human Interactome. *Cell* 2015. doi: 10.1016/j.cell.2015.06.043.
18. Moroishi T, Hansen CG, Guan KL. The emerging roles of YAP and TAZ in cancer. *Nat Rev Cancer* 2015. doi: 10.1038/nrc3876.
19. Pobbati AV, Hong W. Emerging roles of TEAD transcription factors and its coactivators in cancers. *Cancer Biology and Therapy* 2013. doi: 10.4161/cbt.23788.
20. Knight JF, Shepherd CJ, Rizzo S, *et al*. TEAD1 and c-Cbl are novel prostate basal cell markers that correlate with poor clinical outcome in prostate cancer. *Br J Cancer* 2008. doi: 10.1038/sj.bjc.6604774.
21. Liu Y, Wang G, Yang Y, *et al*. Increased TEAD4 expression and nuclear localization in colorectal cancer promote epithelial-mesenchymal transition and metastasis in a YAP-independent manner. *Oncogene* 2016. doi: 10.1038/onc.2015.342.
22. Han W, Jung EM, Cho J, *et al*. DNA copy number alterations and expression of relevant genes in triple-negative breast cancer. *Genes Chromosom* 2008. doi: 10.1002/gcc.20550.
23. Landin Malt A, Cagliero J, Legent K, *et al*. Alteration of TEAD1 expression levels confers apoptotic resistance through the transcriptional up-regulation of Livin. *PLoS One* 2012. doi: 10.1371/journal.pone.0045498.
24. Hucl T, Brody JR, Gallmeier E, *et al*. High cancer-specific expression of mesothelin (MSLN) is attributable to an upstream enhancer containing a transcription enhancer factor-dependent MCAT motif. *Cancer Res* 2007. doi: 10.1158/0008-5472.CAN-07-0474.
25. Zanconato F, Forcato M, Battilana G, *et al*. Genome-wide association between YAP/TAZ/TEAD and AP-1 at enhancers drives oncogenic growth. *Nat Cell Biol* 2015. doi: 10.1038/ncb3216.
26. Liu X, Li H, Rajurkar M, *et al*. Tead and AP1 coordinate transcription and motility. *Cell Rep* 2016. doi: 10.1016/j.celrep.2015.12.104.
27. Verfaillie A, Imrichova H, Atak ZK, *et al*. Decoding the regulatory landscape of melanoma reveals TEADS as regulators of the invasive cell state. *Nat Commun* 2015. doi: 10.1038/ncomms7683.
28. Pobbati AV, Han X, Hung AW, *et al*. Targeting the central pocket in human transcription factor TEAD as a potential cancer therapeutic strategy. *Structure* 2015. doi: 10.1016/j.str.2015.09.009.
29. Noland CL, Gierke S, Schnier PD, *et al*. Palmitoylation of TEAD transcription factors is required for their stability and function in hippo pathway signaling. *Structure* 2016. doi: 10.1016/j.str.2015.11.005.

AQ6

30. Chan P, Han X, Zheng B, *et al*. Autopalmitoylation of TEAD proteins regulates transcriptional output of the hippo pathway. *Nat Chem Biol* 2016. doi: 10.1038/nchembio.2036.
31. Jiao S, Wang H, Shi Z, *et al*. A peptide mimicking VGLL4 function acts as a YAP antagonist therapy against gastric cancer. *Cancer Cell* 2014. doi: 10.1016/j.ccr.2014.01.010.
32. Liu-Chittenden Y, Huang B, Shim JS, *et al*. Genetic and pharmacological disruption of the TEAD-YAP complex suppresses the oncogenic activity of YAP. *Genes Dev* 2012. doi: 10.1101/gad.192856.112.
33. Sastry GM, Adzhigirey M, Day T, *et al*. Protein and ligand preparation: parameters, protocols, and influence on virtual screening enrichments. *J Comput Aided Mol Des* 2013;**27**(3):221–34.
34. Friesner RA, Murphy RB, Repasky MP, *et al*. Extra precision glide: docking and scoring incorporating a model of hydrophobic enclosure for protein− ligand complexes. *J Med Chem* 2006;**49**(21):6177–96.
35. Halgren TA, Murphy RB, Friesner RA, *et al*. Glide: a new approach for rapid, accurate docking and scoring. 2. Enrichment factors in database screening. *J Med Chem* 2004;**47**(7):1750–9.
36. Shelley JC, Cholleti A, Frye LL, *et al*. Epik: a software program for pK a prediction and protonation state generation for drug-like molecules. *J Comput Aided Mol Des* 2007;**21**(12):681–91.
37. Ammarah U, Kumar A, Pal R, *et al*. Identification of new inhibitors against human great wall kinase using in silico approaches. *Sci Rep* 2018;**8**(1):1–2.
38. Gupta S, Misra G, Chandra Pant M, *et al*. Targeting the epidermal growth factor receptor: exploring the potential of novel inhibitor N-(3-ethynylphenyl)-6, 7-bis (2-methoxyethoxy) quinolin-4-amine using docking and molecular dynamics simulation. *Protein Pept Lett* 2012;**19**(9):955–68.
39. Misra G, Gupta S, Jabalia N. Understanding the interactions of high-mobility group of protein domain B1 with DNA adducts generated by platinum anticancer molecules using in silico approaches. *Interdiscip Sci Computational Life Sci* 2018;**10**(3):476–85.
AQ7 40. *QikProp, version 3.5*. New York, NY: Schrödinger, LLC, 2012.
41. Phillips JC, Braun R, Wang W, *et al*. Scalable molecular dynamics with namd. *J Comput Chem* 2005;**26**:1781–802.
42. Kumar A, Sechi LA, Caboni P, *et al*. Dynamical insights into the differential characteristics of mycobacterium avium subsp. Paratuberculosis peptide binding to hla-drb1 proteins associated with multiple sclerosis. *New J Chem* 2015;**39**:1355–66.
43. Kumar A, Delogu F. Dynamical footprint of cross-reactivity in a human autoimmune t-cell receptor. *Sci Rep* 2017;**7**:42496.
44. Essmann U, Perera L, Berkowitz ML, *et al*. A smooth particle mesh ewald method. *J Chem Phys* 1995;**103**:8577–93.
45. Koukos PI, Glykos NM. Grcarma: a fully automated task-oriented interface for the analysis of molecular dynamics trajectories. *J Comput Chem* 2013;**34**:2310–2.
46. Naïm M, Bhat S, Rankin KN, *et al*. Solvated interaction energy (sie) for scoring protein−ligand binding affinities. 1. Exploring the parameter space. *J Chem Inf Model* 2007;**47**:122–33.
47. Humphrey W, Dalke A, Schulten K. Vmd: visual molecular dynamics. *J Mol Graph* 1996;**14**:33–8.
48. Triballeau N, Acher F, Brabet I, *et al*. Virtual screening workflow development guided by the "receiver operating characteristic" curve approach. Application to high-throughput docking on metabotropic glutamate receptor subtype 4. *J Med Chem* 2005;**48**(7):2534–47.
49. Zou J, Xie HZ, Yang SY, *et al*. Towards more accurate pharmacophore modeling: multicomplex-based comprehensive pharmacophore map and most-frequent-feature pharmacophore model of CDK2. *J Mol Graph Model* 2008;**27**(4):430–8.
50. Ansari A, Ali A, Asif M, *et al*. Review: biologically active pyrazole derivatives. *New J Chem* 2017;**41**:16–41. doi: 10.1039/C6NJ03181A.
51. Saleh NM, El-Gazzar MG, Aly HM, *et al*. Novel anticancer fused Pyrazole derivatives as EGFR and VEGFR-2 dual TK inhibitors. *Front Chem* 2020;**7**:917.
52. Aly HM. Synthesis and antitumor activity of some novel pyrazole and thienopyrimidine derivatives. *Phosphorus, Sulfur, and Silicon* 2009;**185**(1):211–21.
53. Nassar IF, El Farargy AF, Abdelrazek FM. Synthesis and anticancer activity of some new fused pyrazoles and their glycoside derivatives. *J Heterocyclic Chem* 2018;**55**:1709–19.